Arabian Journal of Chemistry (2022) **15**, 103792

King Saud University

Arabian Journal of Chemistry

www.ksu.edu.sa
www.sciencedirect.com

Cytotoxic performance of green synthesized Ag and Mg dual doped ZnO NPs using *Salvadora persica* extract against MDA-MB-231 and MCF-10 cells

Khadijeh Hamidian [a], **Mina Sarani** [b,*], **Mahmood Barani** [c], **Faeze Khakbaz** [d]

[a] *Department of Pharmaceutics, Faculty of Pharmacy, Zabol University of Medical Sciences, Zabol, Iran*
[b] *Zabol Medicinal Plants Research Center, Zabol University of Medical Sciences, Zabol, Iran*
[c] *Medical Mycology and Bacteriology Research Center, Kerman University of Medical Sciences 76169-13555 Kerman, Iran*
[d] *Department of Chemistry, Shahid Bahonar University of Kerman, Kerman, Iran*

Received 27 November 2021; accepted 10 February 2022
Available online 14 February 2022

KEYWORDS

Ag and Mg dual doped ZnO NPs;
Green synthesis;
MTT test;
Breast cancer cells

Abstract In this study, dual doped Zinc oxide nanoparticles consisted of silver and magnesium were prepared by *Salvadora persica* extract. Powder X-ray diffraction (PXRD) analysis displayed the formation of wurtzite ZnO phase nanostructures and dual doped nanoparticles. The morphological observations of scanning electron microscopy (SEM) confirmed the hexagonal morphology of prepared nanoparticles. The Raman scattering of this product exhibited the first and second orders of polar and non-polar modes that are the characteristic bonds of a wurtzite structure. The toxicity effects of synthesized un-doped, as well as Ag and Mg dual doped ZnO NPs on breast cancer cell (MDA-MB-231) and breast normal cell (MCF-10A) lines, were investigated by the means of MTT test. Accordingly, in comparison to the case of silver and magnesium doped zinc oxide nanoparticles, the un-doped ZnO NPs caused a more toxic impact on MDA-MB-231cells. There was a lack of any significant toxicity effects from un-doped and Ag and Mg dual doped ZnO nanoparticles on the experimented normal cell line (MCF-10A). The gathered results were indicative of a lower toxicity effect in doped nanoparticles when compared to un-doped nanoparticles and therefore, it can be stated that the doping of silver and magnesium metals produces more reliable zinc oxide nanoparticles.

1. Introduction

In the present century, one of the concerns of scientists in the field of medical science is to find a definitive solution for the treatment of cancer (Arshad et al., 2021). This disease is recognized as the first cause of death in developed countries and the second in developing countries (Wang et al., 2020). Despite the spread of various therapies, including

* Corresponding author at: Zabol Medicinal Plants Research Center, Zabol University of Medical Sciences, Zabol, Iran.
E-mail address: m.sarani@zbmu.ac.ir (M. Sarani).

Peer review under responsibility of King Saud University.

Production and hosting by Elsevier

https://doi.org/10.1016/j.arabjc.2022.103792
1878-5352

chemotherapy, the prevalence of this disease is growing and the need to discover and produce new combating compounds is one of the major global priorities (Kumari et al., 2016; Rodriguez-Nogales et al., 2018).

Considering this crucial demand for novel and less dangerous treatment methods, the exertion of nanomaterials for diagnosing and treating a number of common cancers emerged as a new approach in this field. Therefore, the application of nanoparticles in food, electronics, and medical industries is expanding. The prepared nanoparticles (less than 100 nm) offer an increased surface-to-volume ratio with enhanced abilities to react with organic and inorganic molecules. The application of nanotechnology in medicine involves the usage of very small particles in the field of diagnosis and treatment of human cancers. In this regard, nanoparticles received more attention for certain objectives such as imaging tumors, displaying cancer biomarkers, and targeted drug delivery (Zugazagoitia et al., 2016; Schirrmacher, 2019). It was indicated by researches that metal nanoparticles are more effective in biological applications than the other nanostructures (Cheng et al., 2021). Some of the most prominent medicinal uses of metal nanoparticles, including zinc oxide nanoparticles, are their applications as drug carriers and cancer cell markers since they are abled to pharmacologically guide and identify cancer cells and cause significant therapeutic effects by activating apoptotic pathways (Miri et al., 2020a; Wiesmann et al., 2020; Zhang et al., 2020; Anjum et al., 2021).

Zinc oxide nanoparticles can be produced through various chemical and physical methods such as sol–gel (Kumar, 2020), hydrothermal (Mohan et al., 2020), and Ultrasonic (Luo et al., 2018). However, these methods are not economically viable due to their need for different compounds and facilities while posing numerous risks to the environment; whereas the utilization of environmentally friendly methods procedures can be economically efficient and result in higher rate of production and better quality of nanoparticles (Vijayaraghavan and Ashokkumar, 2017; Sharma et al., 2019). The exertion of plant extracts is one of the most desirable and widely applied methods for producing nanoparticles through an environmentally friendly manner, in which the obtained extract from different parts of plants, including roots, leaves and stems, act as a reducing compound and provide the fabrication of nanoparticles in appropriate sizes and shapes (Jadoun et al., 2021; Agarwal et al., 2017). According to various studies, these nanoparticles exhibited fine cytotoxic power in comparison to the other nanoparticles produced by chemical methods (Hamidian et al., 2021a; Miri et al., 2020b; Miri et al., 2020c; Nazaripour et al., 2021).

The usage of zinc metal for producing oxidized nanoparticles has found many applications in medicine and biomedicine (Anjum et al., 2021). Due to its unique physical and chemical properties, this metal has been used in the production of catalysts, gas sensors, semiconductors, and radiation insulation materials. Various studies indicated the strong ability of zinc oxide nanoparticles to induce apoptosis in cancer cells (Zhang et al., 2020).

Salvadora Persica is a desert plant that grows in the west of Saudi Arabia, Iran, and Africa, which is also recognized by the names of chewing stick, natural Toothbrush, and Meswak. Twigs and roots of *S. Persica* are widely exerted as a cleaning agent for teeth, while there are reports on many other uses of this plant. According to the analysis results of *S. Persica,* it contains trimethylamine, salvadrine alkaloids, chloride, fluoride, silica, sulfur, mustard oil, vitamin C, and gum, as well as a small amount of tannin and sterol (Halawany, 2012; Niazi et al., 2016). In our previous studies, we succeeded in synthesizing CeO_2 (Miri et al., 2020d), Fe_2O_3 (Miri et al., 2020e), and Ni-doped CeO_2 (Miri et al., 2020c) nanoparticles through the application of *S. Persica* extract.

Today, researchers are attempting to dope in ZnO to achieve a better crystallographic quality and optical, electrical, and ferromagnetic properties. In fact, doping is one of the easiest techniques to improve the physicochemical properties of a nanoparticle by adding impure ions to the nanoparticle crystal lattice (Bharat et al., 2019; Medhi et al., 2020). In conformity to the numerous studies performed on the doping of various metals such as cobalt (Kammoun and ghoul., 2021), nickel (Ali et al., 2020), iron (Srinivasulu et al., 2017), etc. to zinc oxide, the doping process succeeded in altering the properties of doped nanoparticles. Therefore in this work, the two metals of magnesium and silver were double-doped to zinc oxide, while the involved nanoparticles were synthesized through a green method by the usage of an aqueous extract of *Salvadora persica*. Lastly, in order to evaluate and compare the effects of doped metals on zinc oxide with un-doped zinc oxide nanoparticles, their cytotoxicity impacts on human breast cancer (MDA-MB-231) and normal (MCF-10) cells were investigated by MTT assay.

2. Material and method

2.1. Extraction of *S. persica*

The bark powder of *S. persica* was weighed and added to distilled water (ratio 1:10) to be shaken for 18 h at 150 rpm. Then, the mixture was filtered by a filter paper of Whatman No. 1. The obtained extract was stored in a refrigerator for the upcoming experiments.

2.2. Synthesis of un-doped and dual doped ZnO NPs

The Mg:Ag ratios of 1:1, 1:2, and 1:4 were considered for synthesizing Ag and Mg dual doped ZnO NPs. 10 cc of *S. persica* extract was volumed to 50 cc with distilled water in four Erlenmeyer flasks for preparing an un-doped sample and three samples of dual doped nanoparticles, respectively. Then, zinc nitrate hexahydrate (0.02 M, $Zn(NO_3)_2{\cdot}6H_2O$, Merck) was added to every four Erlenmeyer flasks. Thereafter, magnesium nitrate hexahydrate ($Mg(NO_3)_2{\cdot}6H_2O$, Merck), and silver nitrate ($AgNO_3$, Merck) was added to the solutions according to the specified ratios , respectively, to be mixed by a heater stirrer at 70 °C for 3 h. In the following, the samples were dried in an oven of 80 °C for 24 h and the resulting raw material was calcined at 600 °C for 2 h. The un-doped, magnesium, and silver dual doped ZnO NPs were labeled as ZnO, Mg/Ag1-ZnO, Mg/Ag2-ZnO, and Mg/Ag4-ZnO, respectively (Fig. 1).

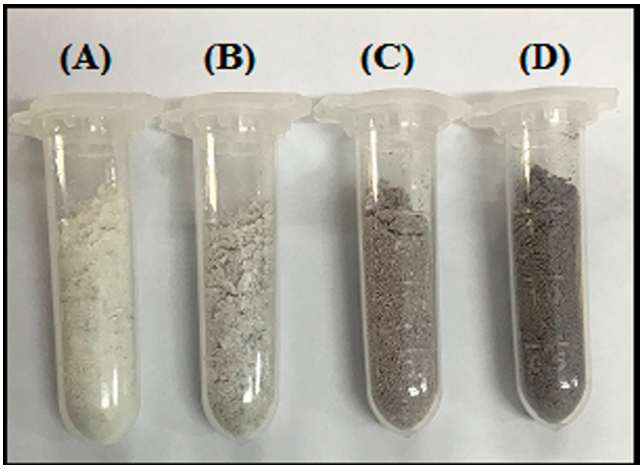

Fig. 1 Images of powders of (A) ZnO, (B) Mg/Ag1-ZnO, (C) Mg/Ag2-ZnO, and (D) Mg/Ag4-ZnO nanoparticles obtained by using *S. persica*.

2.3. Characterization

The morphology and structure of synthesized nanoparticles were investigated through the usage of different characterization methods. The crystalline structure of synthesized nanoparticles was characterized through powder X-ray diffractometer (PXRD, Netherlands, PANalyticalX'Pert PRO MPD system, Cu Kα). In addition, ultraviolet and visible absorption were used to measure the intensity of light at different wavelengths caused by UV–Vis radiation and those that stimulate bonded electrons (UV–Vis, Rayleighuv-2100, Chine). Raman spectroscopy is an analytical technique, in which scattered light is used to measure the vibrational energy modes of a sample, (Raman Takram P50C0R10 device, laser wavelength = 532 nm), while FESEM characterization technique provides important data on surface morphologies such as shapes and sizes of nanoparticles (FESEM, MIRA3 TESCAN, Czech).

2.4. Cytotoxic activity

2.4.1. Cell culture

In order to evaluate the cytotoxicity of our synthesized nanoparticles, we used human breast cancer MDA-MB-231 and normal MCF-10, which were obtained from the Pasteur Institute of Iran and thawed in prior to being cultured. The cells were transferred to Falcon tubes and centrifuged at 833 rpm for 9 min. Once the supernatant was removed, a complete culture medium was added to the cells to have the prepared suspensions poured into flasks. DMEM culture medium was exerted for the process of cell culturing, while 10% fetal bovine serum (FBS), 100 μg/mL of streptomycin, and 100 international units/mL of penicillin was appended to each of the culture mediums to prevent microbial growth. The applied culture medium was incubated under 5% CO_2 at 37 °C for the purpose of proliferating and growing the cells.

2.4.2. MTT assay

Human breast cancer MDA-MB-231 and normal MCF-10A cells were cultured with high glucose DMEM, which was supplemented with 10% fetal bovine serum and 1% penicillin/streptomycin solution, in an incubator (37 °C, 5% CO_2) until the cells of each well reached the count of 10000. The culture medium was replaced with 100 μL of DMEM containing the formulations of different concentrations (1, 10, 50, 100, and 500 μg/mL) to be seeded for another 24 h. Each concentration was composed of three duplications. The culture medium was changed after 24 h along with a replacement of a fresh high glucose DMEM. In the following, 20 μL of 5 mg/mL 3-(4, 5-dimethylthiazol-2-yl)-2, 5-diphenyl tetrazolium bromide (MTT) solution was added to each well to be further incubated for 4 h. Once 100 μL of DMSO was added to each well, the resulting mixture was shaken for about 15 min at room temperature to dissolve its formazan. The optical density (OD) was measured at 570 nm through a microplate reader and the rate of cell viability (VR) was calculated in accordance with the following equation:

$$VR = A/A_0 \times 100\%$$

where A represents the absorbance of cells that were treated with formulations and A_0 refers to the absorbance of control group.

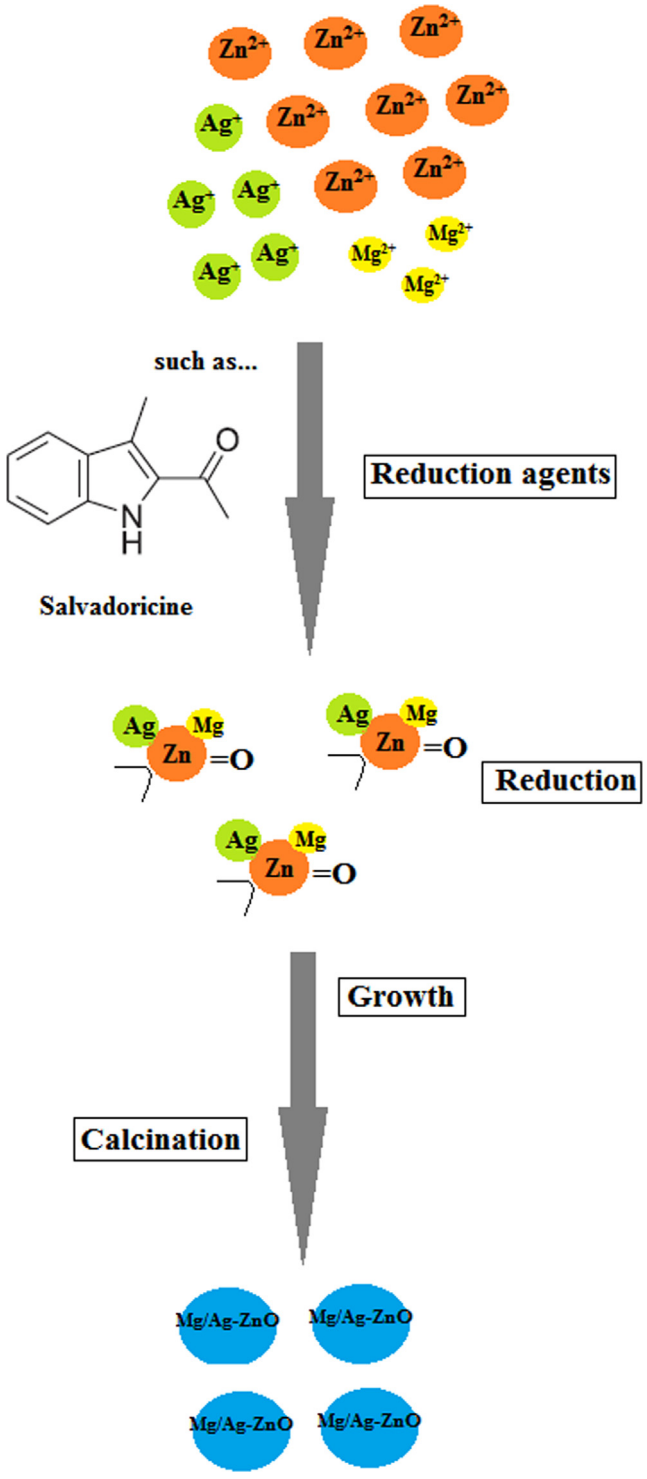

Fig. 2 Synthesis mechanism of formation Mg/Ag-ZnO nanoparticles by using *S. persica* extract.

2.4.3. IC50xxx

The probit test was performed by the usage of SPSS software to calculate the concentrations of drug and nanoparticles that could limit the growth of 50% of cells (IC50), as well as to measure the restriction percentage of cell growth against concentration.

3. Results and discussion

The *S. persica* extract including secondary compounds such as salvadrine alkaloids, chloride, and fluoride, which act as a reducing agent to promote the formation of oxide metallic nanoparticles. The ability of *S. persica* extract to synthesize of metal oxides and metal nanoparticles has been well established in our previous studies. In the continuation of our studies, we were used *S. persica* extract to prepare of double doped metal oxide nanoparticles. The mechanism of nanoparticle synthesis through *S. persica* extract is shown in Fig. 2.

3.1. PXRD analysis

The PXRD pattern of synthesized ZnO, Mg/Ag1-ZnO, Mg/Ag2-ZnO, and Mg/Ag4-ZnO nanoparticles achieved by the usage of *S. persica* is presented in Fig. 3. The observed peaks in non-doped ZnO nanoparticles and Mg/Ag dual doped ZnO nanoparticles was indexed to (100), (002), (101), (102), (110), (103), (200), (112), and (201), which are in accordance with the hexagonal ZnO (JCPDS-36-1451) (Miri et al., 2020a). In conformity to Fig. 3, an increase in Ag ratio resulted in the appearance of silver of doped nanoparticles peaks throughout the PXRD pattern. Considering the lack of observing any other additional peaks, it can be indicated that the synthesized nanoparticles are pure and contain crystalline form. The crystalline size of our synthesized product was calculated through the mentioned Debye–Scherer formula in equation (2).

$$D = K\lambda/\beta cos\theta \quad (2)$$

In which D stands for the crystallite size of nanoparticles, K is the shape factor, λ refers to the wavelength of applied radiation, β would be the full width at half maxima (FWHM) in radians, and θ represents the diffraction angle. The average crystallite size of the synthesized nanoparticles was estimated through the full width at half maxima (FWHM) of the XRD peak (101) by the usage of Debye-Scherer formula, which was reported to be 25.37, 19.73, 28.12, and 33.59 nm for ZnO, Mg/Ag1-ZnO, Mg/Ag2-ZnO, and Mg/Ag4-ZnO nanoparticles, respectively. According to Fig. 3, the doping of Mg and Ag metals to the crystalline network of ZnO nanoparticles resulted in increasing the crystalline size of synthesized doped nanoparticles, which can be the responsible factor for the difference in the ionic radius of zinc atom (1.38 Å) when compared to the doping of silver (1.72 Å) and magnesium (0.66 Å) atoms. As seen, with the increasing of doping percent of silver in ZnO nanoparticles, the crystalline size of samples was increased because of its larger ionic radius.

3.2. FESEM and EDX analysis

Fig. 4 presents the FESEM images of synthesized ZnO, Mg/Ag1-ZnO, Mg/Ag2-ZnO, and Mg/Ag4-ZnO nanoparticles that were obtained by the usage of *S. persica*. Accordingly, ZnO particles contained a hexagonal form while some of them were grown into the shape of rods. All of the particles were displayed in a hexagonal form throughout the FESEM images of doped nanoparticles, which also exhibited the increased size of synthesized particles as a result of doping Ag and Mg metals into the structure of ZnO. The achieved mean particle size distributions of synthesized ZnO, Mg/Ag1-ZnO, Mg/Ag2-ZnO,

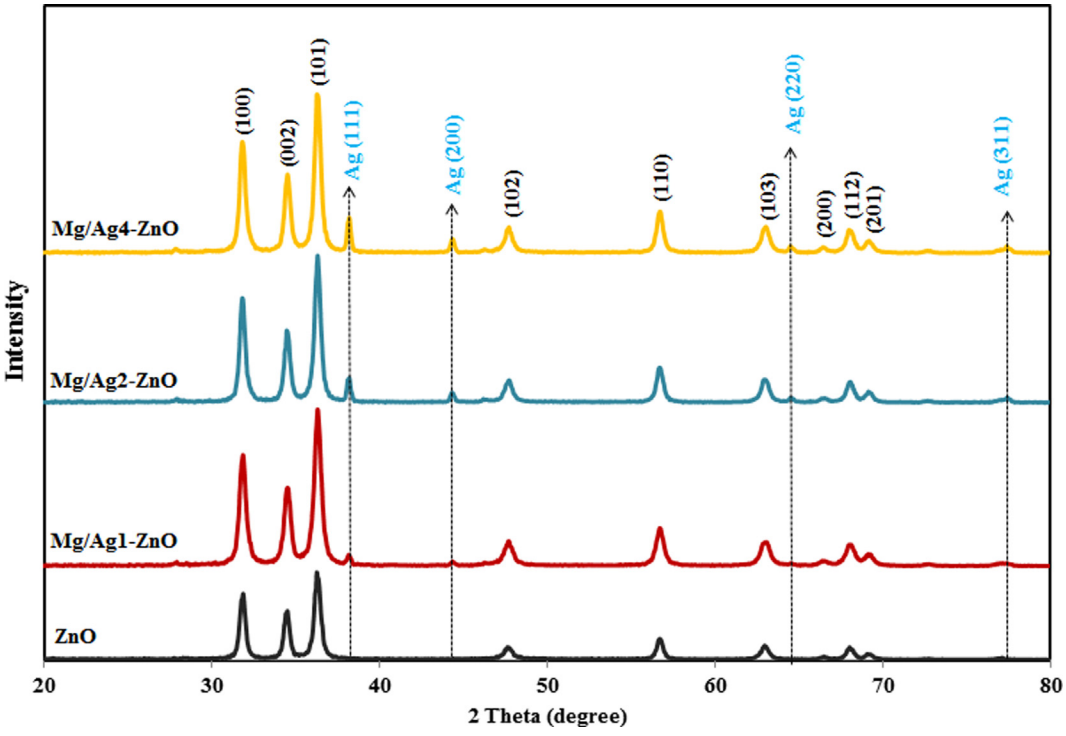

Fig. 3 PXRD pattern of ZnO, Mg/Ag1-ZnO, Mg/Ag2-ZnO, and Mg/Ag4-ZnO nanoparticles obtained by using *S. persica*.

and Mg/Ag4-ZnO nanoparticles, which were estimated to be 36.44, 36.89, 47.92, and 51.45 nm, indicates the satisfying growth of particles as a result of increasing the percentage of doped metals. The EDX profiles of synthesized ZnO and Mg/Ag4-ZnO nanoparticles are demonstrated in Fig. 5. The EDX results confirmed the high-purity content of synthesized nanoparticles along with their composition of Zn and O elements for the case of ZnO and Zn, O, Ag, and Mg elements for the case of Mg/Ag4-ZnO nanoparticles.

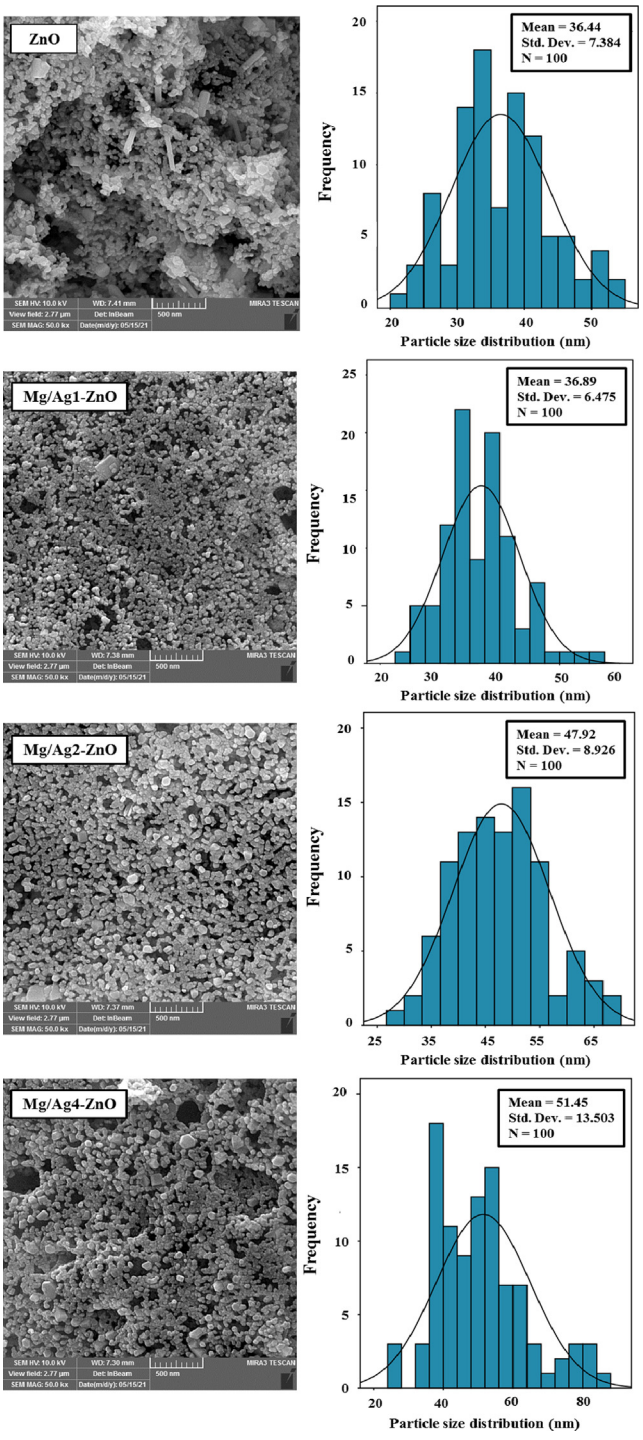

Fig. 4 FESEM images and particle size distribution of ZnO, Mg/Ag1-ZnO, Mg/Ag2-ZnO, and Mg/Ag4-ZnO nanoparticles obtained by using *S. persica*.

3.3. Raman analysis

Raman spectroscopy is an efficient method for identifying molecular structures, since it can determine the rotational and vibrational frequencies, geometric evaluation, and even the symmetry of molecules (Hashemi et al., 2019). According to the group theory, ZnO nanoparticles with a hexagonal wurtzite structure contain a space group of P63mc. Accordingly, the optical modes presented in ZnO wurtzite structure include A1 + 2B2 + E1 + 2E2, which is categorized into A1 + E1 + 2E2 as the active Raman mode, A1 + E1 as the active infrared mode, and 2B1 as the silent Raman mode. E1 and A1 modes are two polar branches that are divided into longitudinal optical (LO) and transverse optical (TO) branches, while A1, E1, and E2 are the first-order Raman active modes. It should be noted that according to Raman law, B1 modes are usually inactive throughout the Raman spectrum and are known as the silent modes (Silambarasan et al., 2014–2015). Fig. 6 displays the Raman spectra of synthesized ZnO, Mg/Ag1-ZnO, Mg/Ag2-ZnO, and Mg/Ag4-ZnO nanoparticles. The main phonon states of hexagonal ZnO nanoparticles appear in 573, 434, 336 and 96 cm^{-1} regions, which correspond to the modes of A1 (LO)-E1 (LO), E2H, A1 (TO), and E2H, respectively. The 2E2L mode is in correlation to the second-order phonon mode that appears in 122 cm^{-1} region. Modes of 3E2H-E2L, E1 (TO) + E2L, 2(E2H-E2L), and A1 (TO) + E1 (TO) + E2L are related to poly-phonon scattering, which appeared in the range of 317, 483, 663 and 1099 cm^{-1}, respectively.

As it is displayed in Fig. 6, the polar and non-polar states faced a significant alteration due to the doping factor (both Ag and Mg) in the matrix of ZnO. The E2H state involves the oxygen motion, sensitivity to internal stress, and characteristics of hexagonal structure of zinc oxide nanoparticles. Caused by the decomposition of impurities and defects, E2H mode faced a sharp decrease in the peak intensities of doped samples, while considering that increasing the doping concentrations of silver and magnesium can induce a steady decrease and expansion in this mode. Furthermore, the appeared polarity of A1 (LO)-E1 (LO) at about 580 cm^{-1} is related to the doping of silver and magnesium, which results in expanding the peak and causing a shift towards lower energies. All variations and extensions of phonon modes were obtained by the scattering contributions outside the center of Brillouin area. The phonon state of A1 (LO) -E1 (LO) is a common sign of interfacial defect of zinc and oxygen vacancy in ZnO network (Khosravi-Gandomani et al., 2014). The doping of Ag and Mg ions with ZnO nanoparticles caused a great increase in the intensity of ZnO Raman peaks. Also, further results confirmed the existence of few defects in the crystallization of ZnO nanoparticles as a result of Ag and Mg ions.

3.4. UV–Vis analysis

UV–Vis technique is a compulsive technique to the optical study of the nanomaterials. The determination of optical data

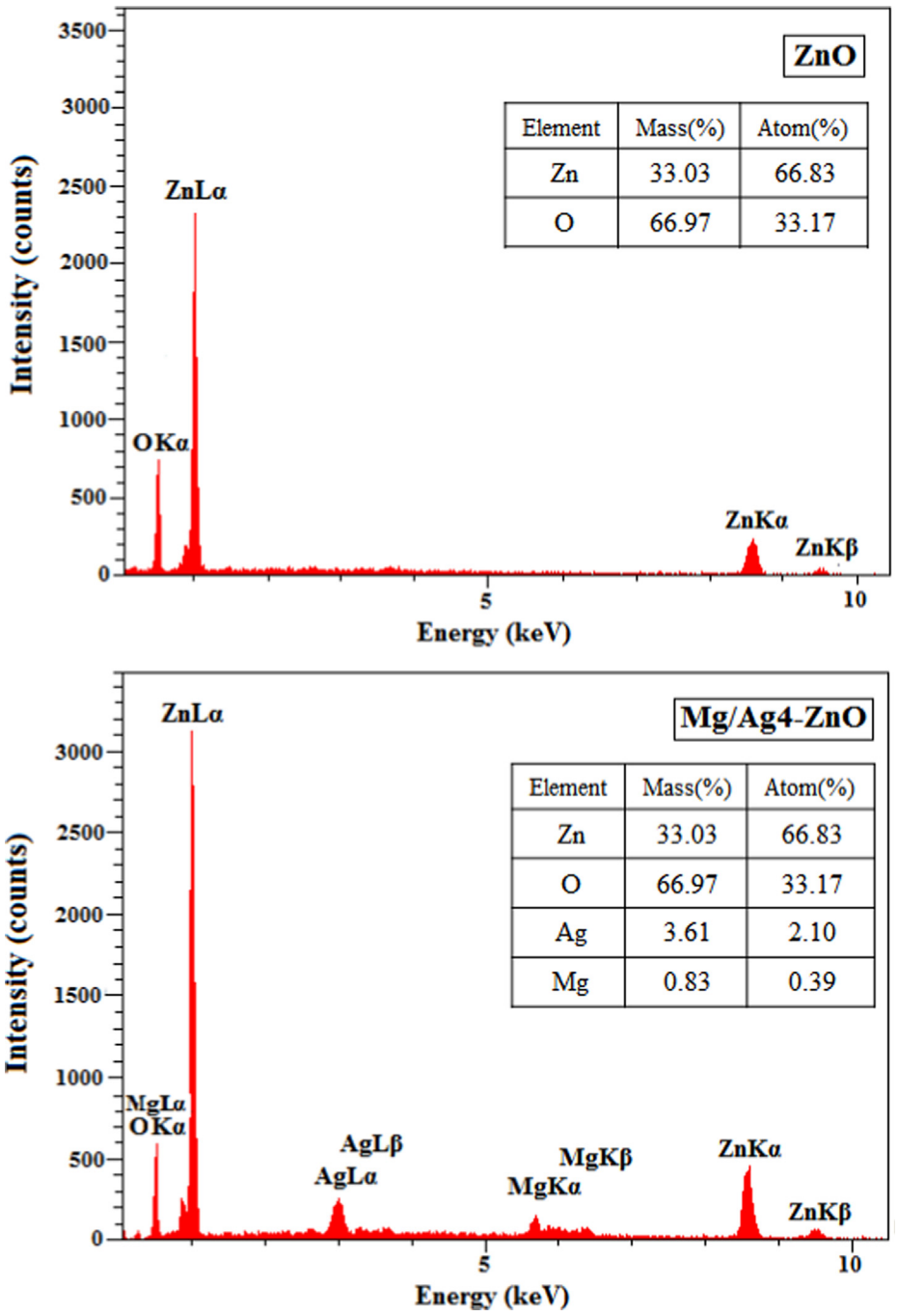

Fig. 5 EDX profiles of ZnO and Mg/Ag4-ZnO nanoparticles obtained by using *S. persica*.

is useful for the applications of nanomaterials for different fields. The UV–Vis absorption spectra of synthesized ZnO, Mg/Ag1-ZnO, Mg/Ag2-ZnO, and Mg/Ag4-ZnO nanoparticles obtained by using *S. persica* are presented in Fig. 7A. The maximum wavelength of ZnO, Mg/Ag1-ZnO, Mg/Ag2-ZnO, and Mg/Ag4-ZnO nanoparticles appeared in the regions of 358, 353, 350, and 348 nm, respectively. An increase in the concentrations of Ag and Mg in ZnO nanoparticles can cause a shift in the position of absorption spectra towards the lower wavelengths, also known as blue shift, which is associated with the induced alteration in the amount of optical band gap (Viswanatha et al., 2004). This blue shift signifies the occurrence of a reduction in crystallization and the effect of quantum confinement. Increasing the electron population during Mg and Ag doping in ZnO leads to quantum constraints and ultimately blue shift in optical absorption behavior (Alanazi et al., 2021).

The DRS spectra of the synthesized ZnO, Mg/Ag1-ZnO, Mg/Ag2-ZnO, and Mg/Ag4-ZnO nanoparticles is presented in Fig. 7B wherein Tauc plot graph (Hamidian et al., 2021b)

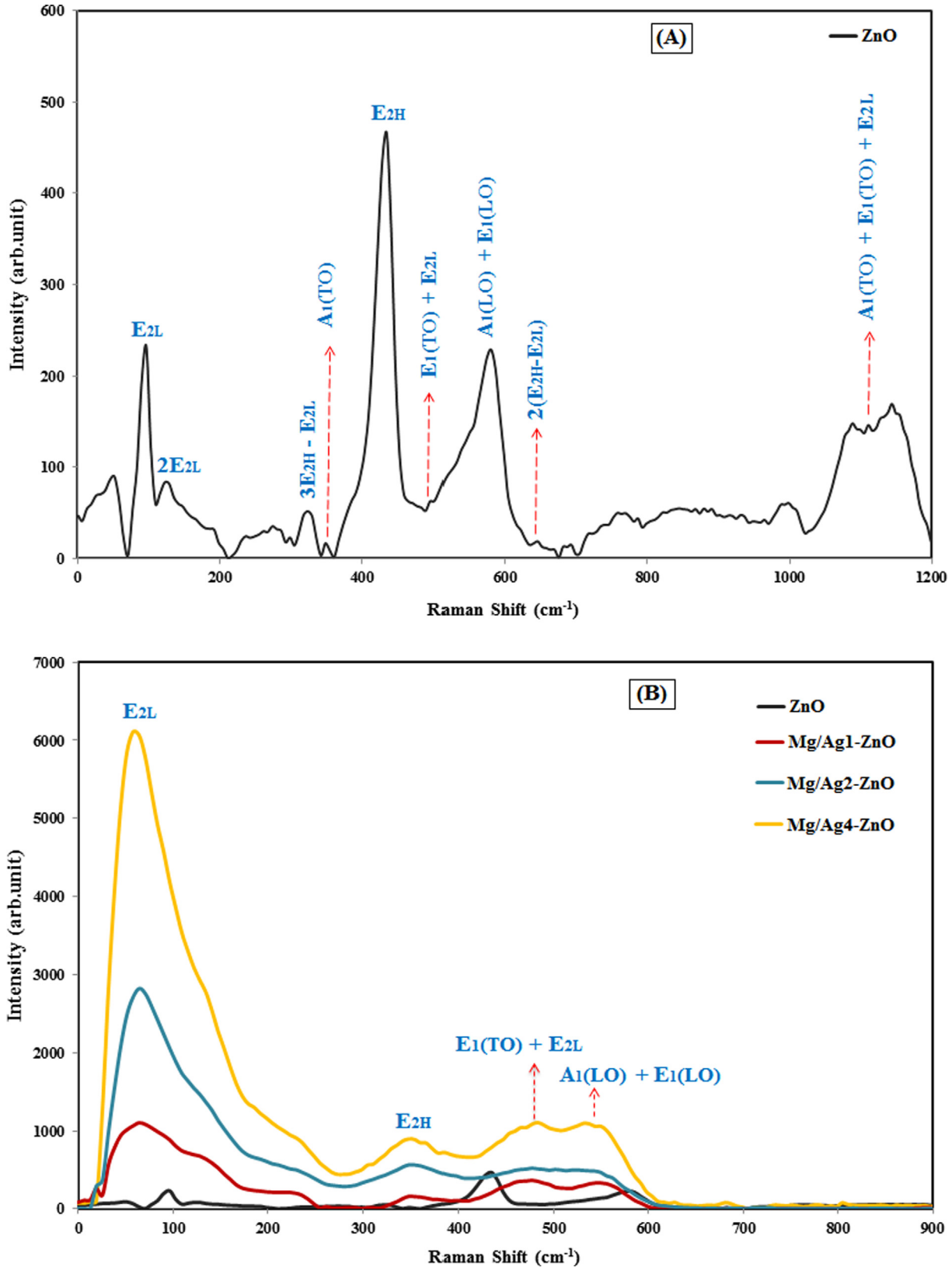

Fig. 6 Raman spectra of (A) ZnO nanoparticles, and (B) ZnO, Mg/Ag1-ZnO, Mg/Ag2-ZnO, and Mg/Ag4-ZnO nanoparticles obtained by using *S. persica*.

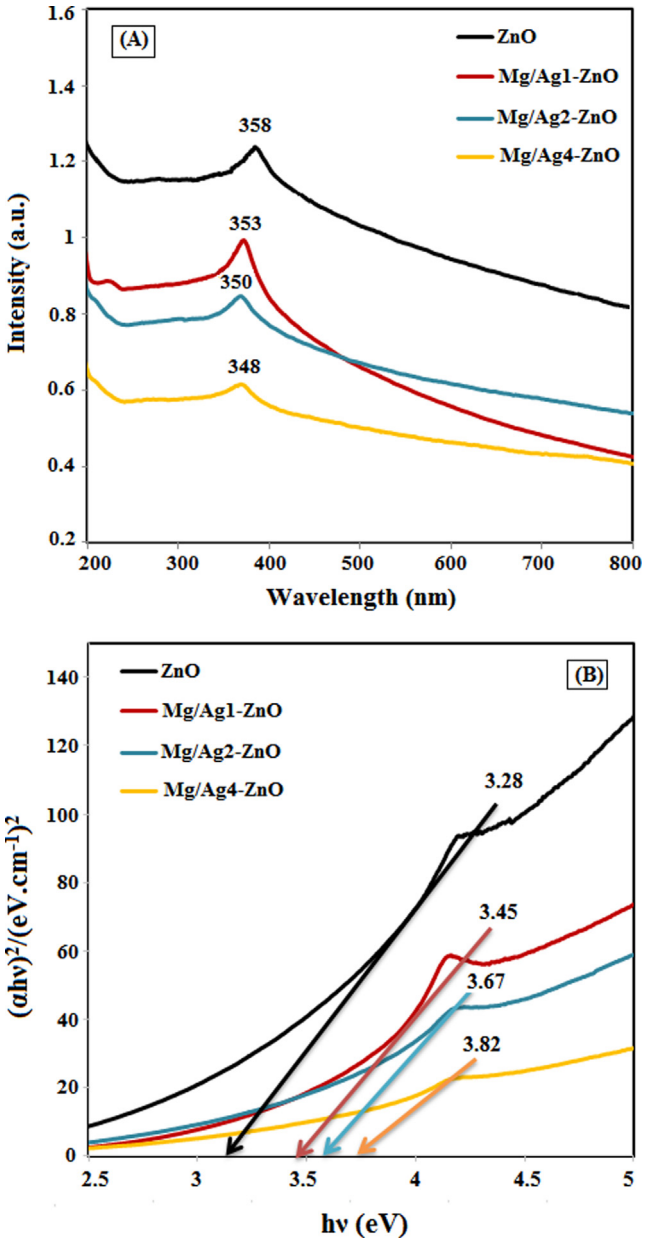

Fig. 7 (A) UV–Vis absorption spectra and (B) DRS of ZnO, Mg/Ag1-ZnO, Mg/Ag2-ZnO, and Mg/Ag4-ZnO nanoparticles obtained by using *S. persica*.

estimated the optical band gap of synthesized nanoparticles. The absorbance spectra display a blue shift with increasing the doping Ag and Mg metals into ZnO structure which leads to an increase in the band gap of doped nanoparticles. The increase in band gap i.e., the blue shift occurs due to the quantum confinement effect (Alanazi et al., 2021); the band gap value being estimated to be 3.28, 3.45, 3.67, and 3.82 eV for ZnO, Mg/Ag1-ZnO, Mg/Ag2-ZnO, and Mg/Ag4-ZnO samples, respectively. It has been observed that as the particle size increases, their band gap increases, which is consistent with PXRD and FESEM results.

3.5. Cytotoxic performance

Recent studies confirmed the importance of metal nanoparticles in medical applications including antimicrobial and anticancer activities. In addition, performing doping processes on metal ions can enhance the biomedical applications of metal oxide nanoparticles by improving their properties (Medhi et al., 2020). For example according to the work of Ahmed *et al,* Ag doped TiO_2 NPs exhibited increased cytotoxicity in cancer cells along with improved biocompatibility in normal cells (Ahamed et al., 2017). Similarly, our previous studies confirmed the increased cytotoxicity of Ni doped CeO_2 NPs in colon cancer cells (HT-29) (Miri et al., 2020c).

In the present study, we examined the cytotoxicity effect of synthesized ZnO, Mg/Ag1-ZnO, Mg/Ag2-ZnO, and Mg/Ag4-ZnO nanoparticles obtained by using *S. persica* against breast cancer cells (MDA-MB-231) and breast normal cells (MCF-10A). Cells were exposed for 24 h at different concentrations (1–500 µg/mL) of un-doped and dual doped ZnO nanoparticles by the means of MTT assay (Fig. 7). According to Fig. 8A, the un-doped and Ag and Mg dual doped ZnO nanoparticles lacked any signs of significant toxicity impacts on the normal cell line (MCF-10A). Doped nanoparticles displayed an almost comparable toxicity effect to that of un-doped nanoparticles, while an increase in the concentrations of doped and un-doped nanoparticles did not cause any significant toxicity impact. The results of analyzing the cytotoxic activity of synthesized nanoparticles on breast cancer cell line (MDA-MB-231) are presented in Fig. 8B. According to observations, the effect of cytotoxicity was intensified as the concentration was increase, which became significant at a concentration of 500 µg/mL. The cytotoxic effect of un-doped nanoparticles was relatively higher than that of doped nanoparticles and therefore, it can be stated that the doping of silver and magnesium caused a relative reduction in the induced cytotoxicity. These results suggested that the synthesized nanoparticles caused the required cytotoxicity in cancer cells while being tolerable towards normal cells.

The amazing effects of green synthesized silver NPs on cancer cells were mentioned in the work of many authors. For example, Swamy *et al* reported the successful synthesis of silver nanoparticles through the application of *Leptadenia reticulata* leaf extract. Accordingly, the performed MTT assay revealed a dose-dependent decrease in cell viability, while microscopic observations displayed a distinct cellular morphological alteration that was indicative of unhealthy cells, and the control appeared in a normal state (Kumara Swamy et al., 2015). In addition, an increase in the number of propidium iodide positive cells was observed in the maximum concentration. Furthermore, another study evaluated the anticancer activity of ZnO nanopowders that was prepared through a solution combustion method by the usage of bio fuels *Punica granatum* and *Tamarindus indica*. Considering the obtained viability values, the prepared ZnO nanopowders through green synthesis at the highest concentrations used in our studies (100 µg/mL), whereas the commercial ZnO nanopowder was able to achieve around 66% of cell viability (Prashanth et al., 2015).

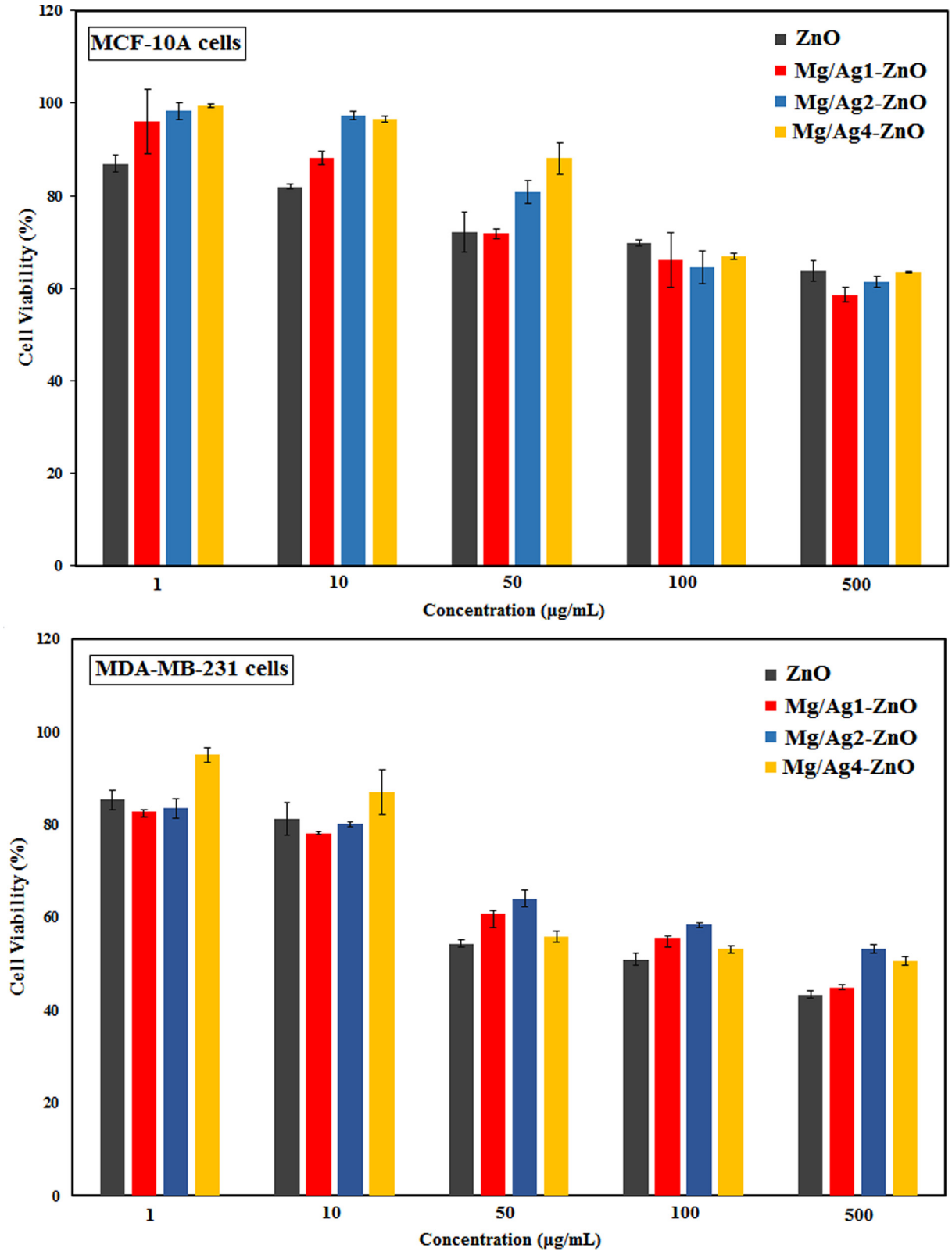

Fig. 8 The cytotoxic activity of ZnO, Mg/Ag1-ZnO, Mg/Ag2-ZnO, and Mg/Ag4-ZnO nanoparticles obtained by using *S. persica*.

4. Conclusion

Un-doped and Ag and Mg dual doped ZnO NPs were synthesized through a facile green method by exerting the extract of *S. persica*. The obtained PXRD spectra displayed the hexagonal phase of un-doped and dual doped ZnO NPs. SEM mapping demonstrated the homogeneous distribution of Ag and Mg in ZnO with high-quality lattice fringes while lacking any distortions. According to cytotoxicity studies, the un-doped ZnO NPs caused a higher toxicity effect on breast cancer cells (MDA-MB-231) than the dual doped ZnO NPs, whereas the synthesized nanoparticles were incapable of inducing any significant toxicity impacts on the normal cell line (MCF-10A). Considering how the toxicity effect of doped nanoparticles was observed to be slightly less than the non-doped nanoparticles, it can be stated that the doping of silver and magnesium metals results in the fabrication of more reliable zinc oxide nanoparticles. This attempt can stand as a useful approach due to the cosmetic and even industrial applications of zinc oxide nanoparticles.

Declaration of Competing Interest

The authors declare that they have no known competing financial interests or personal relationships that could have appeared to influence the work reported in this paper.

References

Agarwal, H., Kumar, S.V., Rajeshkumar, S., 2017. A review on green synthesis of zinc oxide nanoparticles – an eco-friendly approach. Res. Effi. Technol. 3 (4), 406–413.

Ahamed, M., Majeed Khan, M.A., Akhtar, M.J., Alhadlaq, H.A., Alshamsan, A., 2017. Ag-doping regulates the cytotoxicity of TiO_2 nanoparticles via oxidative stress in human cancer cells. Sci. Rep. 7, 17662.

Alanazi, H.S., Ahmad, M., Alharthi, F.A., 2021. Synthesis of Gd/N co-doped ZnO for enhanced UV-vis and direct solar-light-driven photocatalytic degradation. RSC. Adv. 1, 10194.

Ali, M.Y., Khan, M.K.R., Tanveer Karim, A.M.M., Mozibur Rahman, M., Kamruzzaman, M., 2020. Effect of Ni doping on structure, morphology and opto-transport properties of spray pyrolised ZnO nano-fiber. Heliyon. 6, (3) e03588.

Anjum, S., Hashim, M., Malik, S.A., Khan, M., Lorenzo, J.M., Abbasi, B.H., Hano, C., 2021. Recent Advances in Zinc Oxide Nanoparticles (ZnO NPs) for Cancer Diagnosis, Target Drug Delivery, and Treatment. Cancers. 13(18) (2021) 4570.

Arshad, R., Pal, K., Sabir, F., Rahdar, A., Bilal, M., Shahnaz, G., Kyzas, G.Z., 2021. A review of the nanomaterials use for the diagnosis and therapy of salmonella typhi. J. Mol. Stru. 11, 129928.

Bharat, T.C., Shubham, S., H.S., Mondal, Gupta, Singh, P.K., Das, A. K., 2019. Synthesis of Doped Zinc Oxide Nanoparticles: A Review. Mater. Today. Proc. 11, 767-775.

Cheng, Z., Li, M., Dey, R., Chen, Y., 2021. Nanomaterials for cancer therapy: current progress and perspectives. J. Hematol. Oncol. 14 (85), 1–27.

Halawany, H.S., 2012. A review on miswak (*Salvadora persica*) and its effect on various aspects of oral health. Saudi. Dent. J. 24 (2), 63–69.

Hamidian, K., Saberian, M.R., Miri, A., Sharifi, F., Sarani, M., 2021a. Doped and un-doped cerium oxide nanoparticles: biosynthesis, characterization, and cytotoxic study. Ceram. Intern. 47 (5), 13895–13902.

Hamidian, K., Rigi, A.H., Najafidoust, A., Sarani, M., Miri, A., 2021b. Study of photocatalytic activity of green synthesized nickel oxide nanoparticles in the degradation of acid orange 7 dye under visible light. Bioproc. Biosyst. Eng. 44, 2667–2678.

Hashemi, A., Krasheninnikov, A.V., Puska, M., Komsa, H.P., 2019. Efficient method for calculating Raman spectra of solids with impurities and alloys and its application to two-dimensional transition metal dichalcogenides. Phys. Rev. Mater. 3, 023806.

Jadoun, S., Arif, R., Jangid, N.K., Meena, R.K., 2021. Green synthesis of nanoparticles using plant extracts: a review. Environ. Chem. Lett. 19, 355–374.

Kammoun, S., ghoul, J.E., 2021. Structural and optical investigation of Co-doped ZnO nanoparticles for nanooptoelectronic devices. . 32, 7215-7225.

Khosravi-Gandomani, S., Yousefi, R., Jamali-Sheini, F., MingHuang, N., 2014. Optical and electrical properties of *p*-type Ag-doped ZnO nanostructures. Ceram. Int. 40 (6), 7957–7963.

Kumar, A., 2020. Sol gel synthesis of zinc oxide nanoparticles and their application as nano-composite electrode material for super-capacitor. J. Mol. Struct. 1220, 128654.

Kumari, P., Ghosh, B., Biswas, S., 2016. Nanocarriers for cancer-targeted drug delivery. J Drug Target. 24, 179–191.

Kumara Swamy, M., Sudipta, K.M., Jayanta, K., Balasubramanya, S., 2015. The green synthesis, characterization, and evaluation of the biological activities of silver nanoparticles synthesized from *Leptadenia reticulata* leaf extract. Appl. Nanosci. 5, 73–81.

Luo, Z., Zhu, M., Guo, M., Lian, Z., Tong, W., Wang, J., Zhang, B., Wei, W., 2018. Ultrasonic-assisted dispersion of ZnO nanoparticles and its inhibition activity to Trichoderma viride. J. Nanosci. Nanotechnol. 18 (4), 2352–2360.

Medhi, R., Marquez, M.D., Lee, T.R., 2020. Visible-light-active doped metal oxide nanoparticles: review of their synthesis, properties, and applications. ACS Appl. Nano. Mater. 3 (7), 6156–6185.

Miri, A., Khatami, M., Ebrahimy, O., Sarani, M., 2020a. Cytotoxic and antifungal studies of biosynthesized zinc oxide nanoparticles using extract of Prosopis farcta fruit. Green. Chem. Lett. Rev. 13 (1), 27–33.

Miri, A., Akbarpour Birjandi, S., Sarani, M., 2020b. Survey of cytotoxic and UV protection effects of biosynthesized cerium oxide nanoparticles. J. biochem. Mol. Toxicol. 34, (6) e22475.

Miri, A., Sarani, M., Khatami, M., 2020c. Nickel-doped cerium oxide nanoparticles: biosynthesis, cytotoxicity and UV protection studies. Rsc. Adv. 10 (7), 3967–3977.

Miri, A., Darroudi, M., Sarani, M., 2020d. Biosynthesis of cerium oxide nanoparticles and its cytotoxicity survey against colon cancer cell line. Appl. Organomet. Chem. 34, (1) e5308.

Miri, A., Khatami, M., Sarani, M., 2020e. Biosynthesis, magnetic and cytotoxic studies of hematite nanoparticles. J. Inorg. Organomet. Polym. Mater. 30 (3), 767–774.

Mohan, S., Vellakkat, M., Aravind, R., Reka, U., 2020. Hydrothermal synthesis and characterization of Zinc Oxide nanoparticles of various shapes under different reaction conditions. Nano. Ex. 1, (3) 030028.

Nazaripour, E., Mousazadeh, F., Moghadam, M.D., Najafi, K., Borhani, F., Sarani, M., Ghasemi, M., Rahdar, A., Iravani, S., Khatami, M., 2021. Biosynthesis of lead oxide and cerium oxide nanoparticles and their cytotoxic activities against colon cancer cell line. Inorg. Chem. Commun. 131, 108800.

Niazi, F., Naseem, M., Khurshid, Z., Zafar, M.S., Almas, M., 2016. Role of *Salvadora persica* chewing stick (miswak): A natural toothbrush for holistic oral health. Eur. J. Dent. 10 (2), 301–308.

Prashanth, G.K., Prashanth, P.A., Bora, U., Gadewar, M., Nagabhushana, B.M., Ananda, S., Krishnaiah, G.M., Sathyananda, H. M., 2015. In vitro antibacterial and cytotoxicity studies of ZnO nanopowders prepared by combustion assisted facile green synthesis, Karbala. Intl. J. Mod. Sci. 1 (2), 67–77.

Rodriguez-Nogales, C., Gonzalez-Fernandez, Y., Aldaz, A., Couvreur, P., Blanco-Prieto, M.J., 2018. Nanomedicines for Pediatric Cancers. ACS Nano. 12, 7482–7496.

Schirrmacher, V., 2019. From chemotherapy to biological therapy: a review of novel concepts to reduce the side effects of systemic cancer treatment. Int. J. Oncol. 54 (2), 407–419.

Sharma, D., Kanchi, S., Bisetty, K., 2019. Biogenic synthesis of nanoparticles: a review. Arab. J. Chem. 12 (8), 3576–3600.

Silambarasan, M., Saravanan, S., Soga, T., 2014–2015.. Raman and photoluminescence studies of Ag and Fe-doped ZnO nanoparticles. Int. J. ChemTech. Res. 7 (3), 1644–1650.

Srinivasulu, T., Saritha, K., Ramakrishna Reddy, K.T., 2017. Synthesis and characterization of Fe-doped ZnO thin films deposited by chemical spray pyrolysis. Mod. Electron. Mater. 3 (2), 76–85.

Vijayaraghavan, K., Ashokkumar, T., 2017. Plant-mediated biosynthesis of metallic nanoparticles: a review of literature, factors affecting synthesis, characterization techniques and applications. J. Environ. Chem. Eng. 5 (5), 4866–4883.

Viswanatha, R., Sapra, S., Gupta, S.S., Satpati, B., Satyam, P.V., Dev, B.N., Sarma, D.D., 2004. Synthesis and characterization of Mn-doped ZnO nanocrystals. J. Phys. Chem. B. 108 (20), 6303–6310.

Wang, S.Y., Hu, H.Z., Qing, X.C., Zhang, Z.C., Shao, Z.W., 2020. Recent advances of drug delivery nanocarriers in osteosarcoma treatment. J. Cancer. 11, 69.

Wiesmann, N., Tremel, W., Brieger, J., 2020. Zinc oxide nanoparticles for therapeutic purposes in cancer medicine. J. Mater. Chem. B. 8, 4973–4989.

Zhang, T., Du, E., Liu, Y., Cheng, J., Zhang, Z., Xu, Y., Qi, S., Chen, Y., 2020. Anticancer effects of zinc oxide nanoparticles through altering the methylation status of histone on bladder cancer cells. Int. J. Nanomedicine. 15, 1457–1468.

Zugazagoitia, J., Guedes, C., Ponce, S., Ferrer, I., Molina-Pinelo, S., Paz-Ares, L., 2016. Current challenges in cancer treatment. Clin. Ther. 38 (7), 1551–1566.